Langmuir

Article

pubs.acs.org/Langmuir

Molecular Junctions Based on SAMs of Cruciform Oligo(phenylene ethynylene)s

Zhongming Wei,[†] Tao Li,[†] Karsten Jennum,[†] Marco Santella,[†] Nicolas Bovet,[†] Wenping Hu,[‡] Mogens Brøndsted Nielsen,[†] Thomas Bjørnholm,[†] Gemma C. Solomon,[†] Bo W. Laursen,*[,†] and Kasper Nørgaard*[,†]

[†]Nano-Science Center & Department of Chemistry, University of Copenhagen, Universitetsparken 5, DK-2100 Copenhagen, Denmark

[‡]Beijing National Laboratory for Molecular Sciences, Key Laboratory of Organic Solids, Institute of Chemistry, Chinese Academy of Sciences, Beijing 100190, China

Supporting Information

ABSTRACT: Cruciform oligo(phenylene ethynylene)s (OPEs) with an extended tetrathiafulvalene (TTF) donor moiety (OPE5–TTF and OPE3–TTF) and their simple analogues (OPE5-S and OPE3) without conjugated substituents were used to form high-quality self-assembled monolayers (SAMs) on ultraflat gold substrates. Molecular junctions based on these SAMs were investigated using conducting-probe atomic force microscopy (CP-AFM). The TTF substituent changes the molecular orbital energy levels and decreases the HOMO–LUMO energy gap, resulting in a 9-fold increase in conductance for both TTF cruciform OPEs compared to the unsubstituted analogues. The difference in electrical transport properties of the SAMs was reproduced by the theoretical transport calculations for the single molecules.

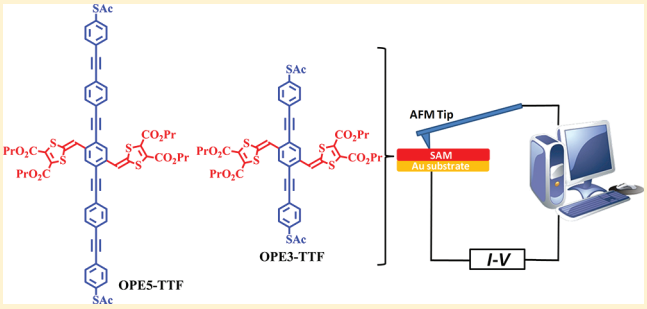

INTRODUCTION

Since the first theoretical simulation of a single molecule as the active part of a rectifier in 1974,[1] molecular electronics has attracted tremendous attention. Decades of research have provided insight into the relationship between molecular structure and intrinsic charge transport properties,[2−5] and theoretical calculations have proven helpful in understanding and explaining the structure−property relations.[6] One of the most difficult challenges for molecular electronics is formation of nanogap electrodes separated by a well-defined molecular structure.[7] Several strategies have been applied to address this problem: discrete molecules[2] and small groups of molecules[6] can be measured using a variety of different methods, such as scanning tunneling microscopy (STM),[8] mechanically controllable break junctions (MCBJs),[9] nanogaps from angled shadow mask deposition,[10] conducting probe-atomic force microscopy (CP-AFM),[11] conducting mercury[12] or EGaIn drops,[13] and others.[14] Among these methods, CP-AFM, which use the AFM tip as a top electrode, has proved to be an efficient and convenient way to measure monolayer molecular junctions on the order of a few hundred molecules.[15] Frisbie et al. applied the CP-AFM to characterize the conductance of self-assembled monolayers (SAMs) based on thiols[16] and conjugated molecular wires of different length.[11,17,18]

Molecular wires, such as oligo(phenylene ethynylene)s (OPEs), have been utilized in molecular electronics for approximately 20 years.[19−21] With the rigid, highly conjugated, and conductive backbone, OPEs have exhibited many interesting properties when residing in molecular junctions, including effects of chemical substitution. Chemical substituents can significantly modify the molecular properties and orbital level alignment and, consequently, change the conductance and device performance (such as molecular switching and thermoelectrical properties) of single-molecule electronics.[22−25] Tour et al. reported that nitroamine-substituted OPE3 showed negative differential resistance[26] and conductance switching.[27] Tao et al. reported that a nitro substituent decreases the conductance of OPE3 by a factor of 2.[28] Interestingly, Calame and co-workers also reported that solubilizing side groups on OPE3 do not noticeably influence the single-molecule conductance.[29] Thus, understanding the effects of chemical substitution is important for the design of new molecules for functional molecular electronics.

As both OPE and redox-active tetrathiafulvalene (TTF)[17,30] derivatives are interesting molecules for molecular electronics, we became interested in the combination of these two classes of molecules. Our group has previously reported the synthesis of an OPE-cruciform molecules incorporating an extended TTF

Received: November 4, 2011
Revised: January 27, 2012
Published: January 27, 2012

   dx.doi.org/10.1021/la204340n | *Langmuir* 2012, 28, 4016−4023

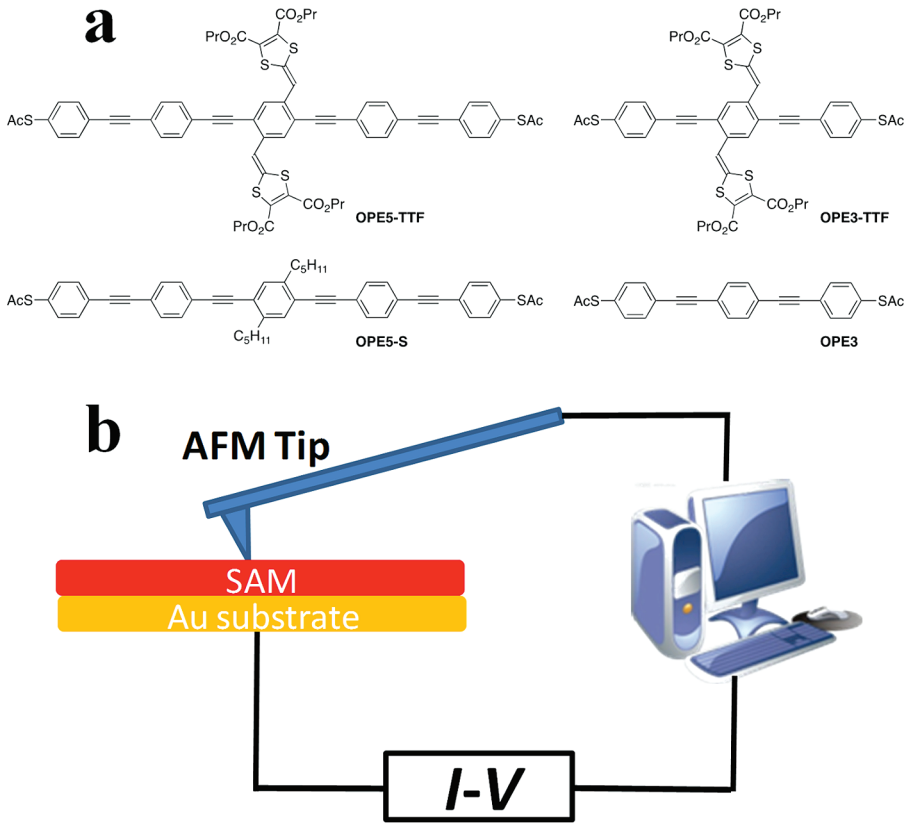

Figure 1. (a) Molecular structures of OPEs and OPE−TTF cruciforms. (b) Schematic illustration of CP-AFM measurement of SAMs in the current study.

donor group into an OPE3 and OPE5 backbone (OPE3−TTF and OPE5−TTF, Figure 1a).[31−33] Herein, we report the studies of molecular junctions based on these cruciform molecules (OPE3−TTF and OPE5−TTF shown in Figure 1a). The cruciform OPEs with acetyl-protected dithiols form high-quality SAMs on Au substrates. These SAMs are characterized by CP-AFM as vertical devices (Figure 1b). The SAMs of OPE5−TTF show 1 order of magnitude higher conductance than its simplified analogue (OPE5-S, Figure 1a) containing only nonconjugated alkyl side chains. At the same time, the SAMs of OPE3−TTF also show higher conductance than OPE3 (Figure 1a, which has been widely used for molecular electronics[28,34] and do not carry any side chains). The difference in electrical properties of the molecules is also investigated theoretically and related to the experimental findings.

RESULTS AND DISCUSSION

The synthesis of the new compound OPE5-S is shown in Scheme 1 (for details see Supporting Information). First, 1,4-dichlorobenzene **1** was converted to the known 1,4-dipentylbenzene **2**[35,36] by a Kumada coupling using conditions described previously for synthesis of 1,4-dihexylbenzene.[37] Subsequent diiodination gave **3** that was then subjected to a palladium-catalyzed cross-coupling reaction with the terminal alkyne **4**[38] to furnish OPE3 **5**. Desilylation provided compound **6**,[39] which in a final cross-coupling reaction with the iodide **7**[31] gave OPE5-S. Synthesis of the cruciform OPE5−TTF was reported previously.[31] OPE3−TTF cruciform was prepared by subjecting the known precursor **8**[31] to a 2-fold palladium-catalyzed cross-coupling reaction with the iodide **7** as shown in Scheme 2 (for details see Supporting Information).

Very recently, Chiechi et al. reported the use of 15% volume triethylamine (Et_3N) as a suitable base to deprotect thiol acetates in THF to obtain high-quality OPE SAMs.[34,40] We used the same solvent to fabricate the SAMs of OPEs. As the length of the active channel in molecular junctions is only the length of the molecule itself (nm), the smoothness of the substrate is highly important in SAM devices. Ultraflat gold substrates were obtained by an annealed template-stripping approach, modified from the methods of Whitesides[41] and Pinkhassik[42] et al. (Figure S1, Supporting Information). This procedure yielded surface roughnesses of 2−3 Å over large areas.

The density and composition of the cruciform OPE SAMs were characterized by cyclic voltammetry (CV) and X-ray photoelectron spectroscopy (XPS).

Figure 2 shows the cyclic voltammograms of an aqueous 5.0 mM $K_3Fe(CN)_6/K_4Fe(CN)_6$ solution recorded with the three cruciform OPE SAMs on Au as electrode. Compared with the bare Au electrode, the peaks for the Fe^{2+}/Fe^{3+} redox signal totally disappears when the OPE5 SAMs cover the Au electrode surface, implying that both the OPE5-S and the OPE5−TTF molecules form high-density SAMs that block access to the Au surface completely. The cruciform OPE5 SAMs were high quality, free of pinholes and defects, and densely packed with coverage close to 100% on the Au surface. For OPE3−TTF SAMs, although the Fe^{2+}/Fe^{3+} redox process was also blocked, the current was slightly larger than the current observed for the two other SAMs. This observation might be a consequence of the shorter backbone of OPE3 in combination with the

dx.doi.org/10.1021/la204340n | *Langmuir* 2012, 28, 4016−4023

Scheme 1. Synthesis of OPE5-S[a]

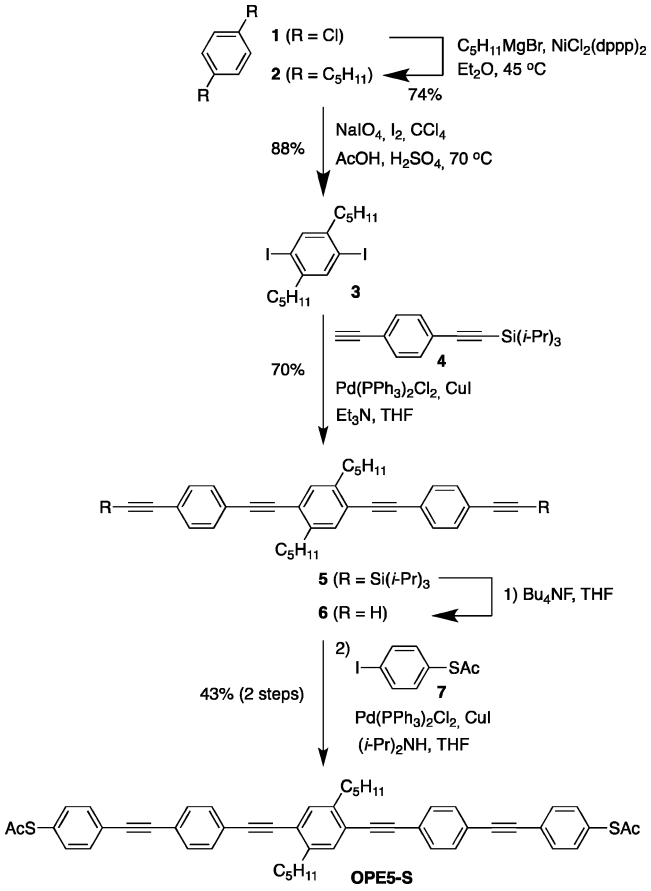

[a]dppp =1,3-bis(diphenylphosphino)propane.

Scheme 2. Synthesis of OPE3−TTF

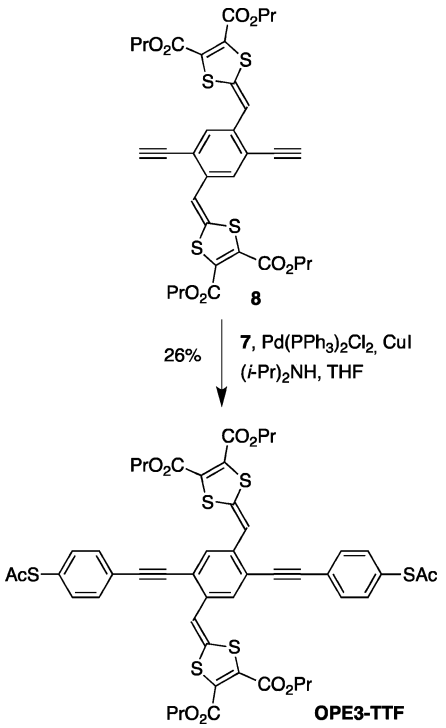

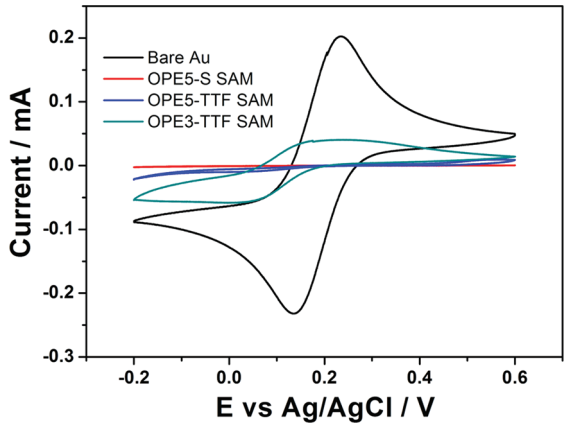

Figure 2. Cyclic voltammograms of bare Au and OPE SAMs on Au.

relatively large side chain. Halik et al. reported that a certain aspect ratio is favorable for forming SAMs with typical chain lengths ranging from 0.5 to 5 nm.[44] As the TTF side chain has a length similar to the OPE3 backbone, the lower aspect ratio OPE3−TTF grow SAMs less readily than the higher aspect ratio OPE5−TTF. The coverage of OPE3−TTF SAM did not reach 100% but was still sufficient for the purpose of the other characterizations as CV measurement is very sensitive to the pinholes.

The structure and quality of the SAMs were also investigated by XPS. By analyzing the intensity ratio of S atoms bound and unbound to Au it could be determined whether the OPE backbone was standing up or lying down on the substrate.[21,34,43] From the XPS spectra of the S2$p_{3/2}$ signals for the OPE5 SAMs (Figure 3) three types of S atoms were identified in the SAMs (i) bound to Au (S−Au, S 2$p_{3/2}$ = 162 eV), (ii) bound to R (S−R, R refer to H/Ac/C(in the TTF group), S 2$p_{3/2}$ = 164 eV), and (iii) oxidized (S═O, S 2$p_{3/2}$ = 168 eV).[43] For OPE5-S, the relative intensity of the peaks for S−Au and S−R showed a ratio of about 1:1 (Figure 3b), which indicates that nearly all the OPE5-S molecules in the SAM are standing up on the Au surface. For the OPE5−TTF and OPE3−TTF SAMs, the situation was complicated by the presence of additional S atoms on the TTF moiety. The ideal ratio for the two types of S atoms should be 1:5 as calculated from the molecular structures; however, the relative intensity of the peaks for S−Au and S−R showed a ratio of about 1:4.2 and 1:3 for OPE5−TTF and OPE3−TTF, respectively (Figure 3a and 3c). This ratio might be a result of increased attenuation[34] of the S−Au signal as it is buried under a larger number of atoms (OPE5−TTF and OPE3−TTF have a much larger side chain than OPE5-S). Nevertheless, the results show that most of the OPE5−TTF and OPE3−TTF molecules in the SAMs are also standing up on the Au surface. These results agree well with other reported OPE SAMs.[34,43] The alignment of cruciform OPEs with the backbone standing up in a SAM is beneficial for electrical measurement of vertical molecular junctions, as the charge carriers can move through the highly conductive and rigid OPE backbones. The thickness of the SAMs was calculated from the attenuation of XPS spectra (for details see Supporting Information).

The transport properties of the SAMs were measured using CP-AFM. Pt/Cr-coated conductive tips were used as the top electrode. Figure 4 shows the *I*−*V* curves of molecular junctions. OPE3 SAM was also fabricated and measured for comparison with OPE3−TTF. Although the molecular

dx.doi.org/10.1021/la204340n | *Langmuir* 2012, 28, 4016−4023

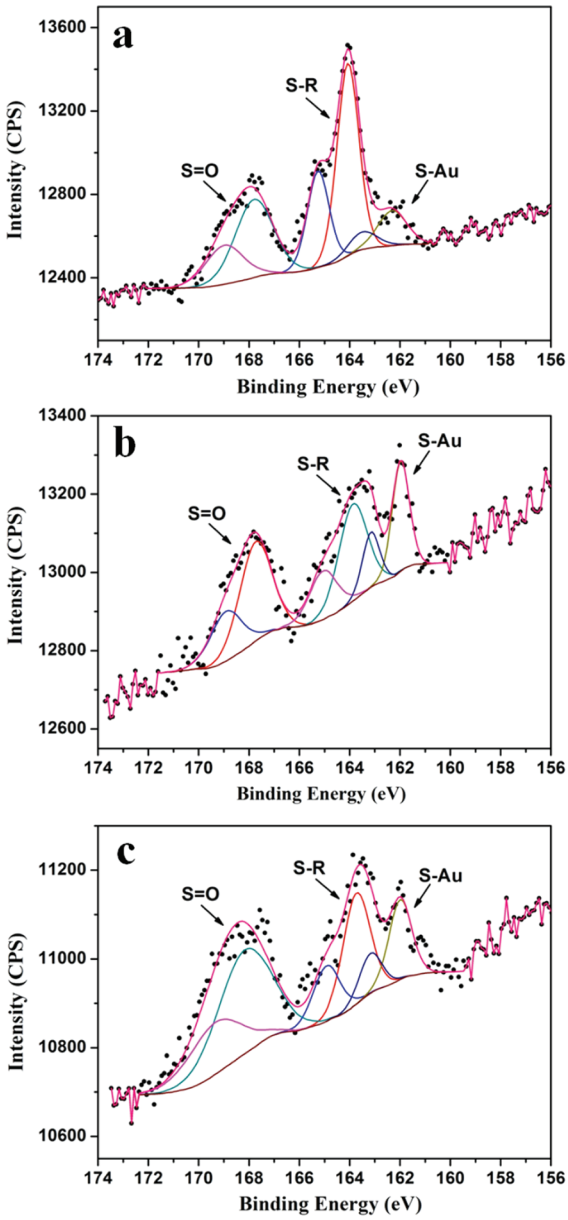

Figure 3. XPS spectra of S2$p_{3/2}$ signals for the cruciform OPE SAMs: (a) OPE5−TTF, (b) OPE5-S, and (c) OPE3−TTF.

junctions are asymmetric due to the different nature of the two metal electrodes (Pt tip and Au surface), all of the four SAMs showed nearly symmetric *I*−*V* characteristics. The resistances were determined over a small voltage range (±0.3 V). TTF-substituted OPE5 (OPE5−TTF SAM, $R = 1.65 \times 10^7$ Ω) showed about 9.3 times lower resistance than its simple analogue (OPE5-S SAM $R = 1.54 \times 10^8$ Ω) bearing only nonconjugated alkyl side chains (Figure 4a). Similarly, Figure 4b shows that the resistance of OPE3−TTF SAM ($R = 1.15 \times 10^6$ Ω) is 8.7 times lower than OPE3 ($R = 9.97 \times 10^6$ Ω). Our *I*−*V* measurements by CP-AFM were calibrated against a dodecanethiol ($C_{12}H_{25}$−SH) SAM (for details see Supporting Information). Herein, we assume OPE5−TTF, OPE5-S, and $C_{12}H_{25}$−SH have molecular areas of 50, 35, and 23 Å^2, respectively. With these areas, the resistance (*R*) of a single molecule can be roughly compared. When calculated at 0.3 V, $R_{C12H25-SH} = 65\,000 \times R_{OPE5-TTF}$, $R_{C12H25-SH} = 4600 \times R_{OPE5-S}$.

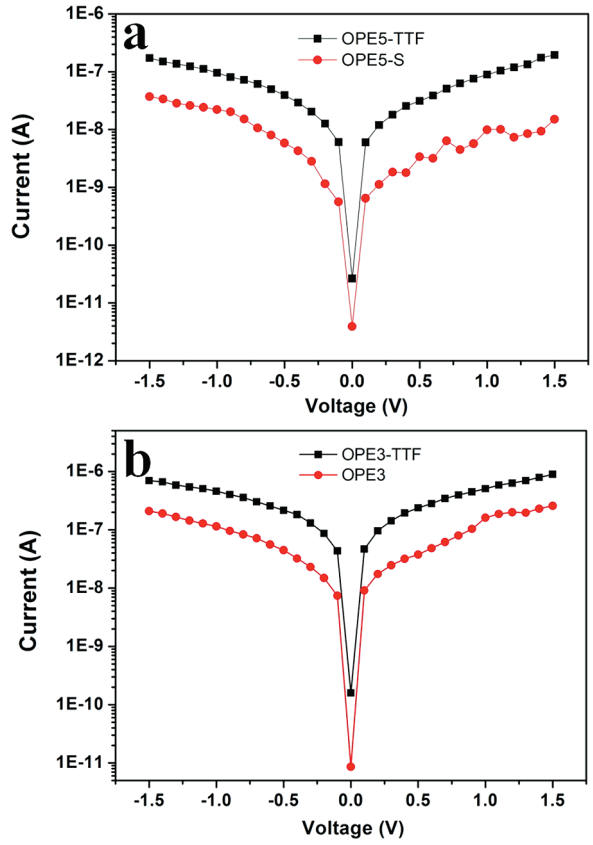

Figure 4. *I*−*V* curves of the molecular junctions based on (a) two OPE5 SAMs and (b) two OPE3 SAMs.

With the same molecular backbone for the two groups of OPEs introduction of the strong electron-donating TTF results in a significant increase in conductance (ca. 14-fold for OPE5-S vs OPE5−TTF). An electron-donating substituent may efficiently increase the energy of the HOMO orbital to more closely match the metal Fermi level.[23] Thus, the transport barrier can be decreased and the conductance of the molecular junction increased. In our case, the alkyl side chain on OPE5-S is also a weak electron donor but much less so than the extended TTF moiety.

For solid-state molecular electronics, a multitude of parameters determine the transport properties. These parameters include molecular length and conformation, electronic coupling between molecules and electrodes, addition energy (U_{add}), contact resistance, and typical quantum mechanical gap between the highest occupied molecular orbital (HOMO) and the lowest unoccupied molecular orbital (LUMO).[4] The two groups of OPEs studied here have the same molecular length and similar SAM thickness. With the same device structure, a significant difference in the junctions, caused by the substitution pattern, is the HOMO and LUMO level. The two OPE5s (or OPE3s) have different HOMO−LUMO gaps and different alignment of the gaps with the electrode Fermi level.

The structure of the isolated OPE molecules were optimized using density functional theory (DFT) in Q-Chem[45] (Table S1, Supporting Information). From the molecular orbital energies, we can see that TTF substituents increase the HOMO level significantly but the LUMO level is not changed much for neither OPE5s nor OPE3s. Thus, the HOMO−LUMO gap of OPE5−TTF (or OPE3−TTF) is smaller than OPE5-S (or

dx.doi.org/10.1021/la204340n | *Langmuir* 2012, 28, 4016−4023

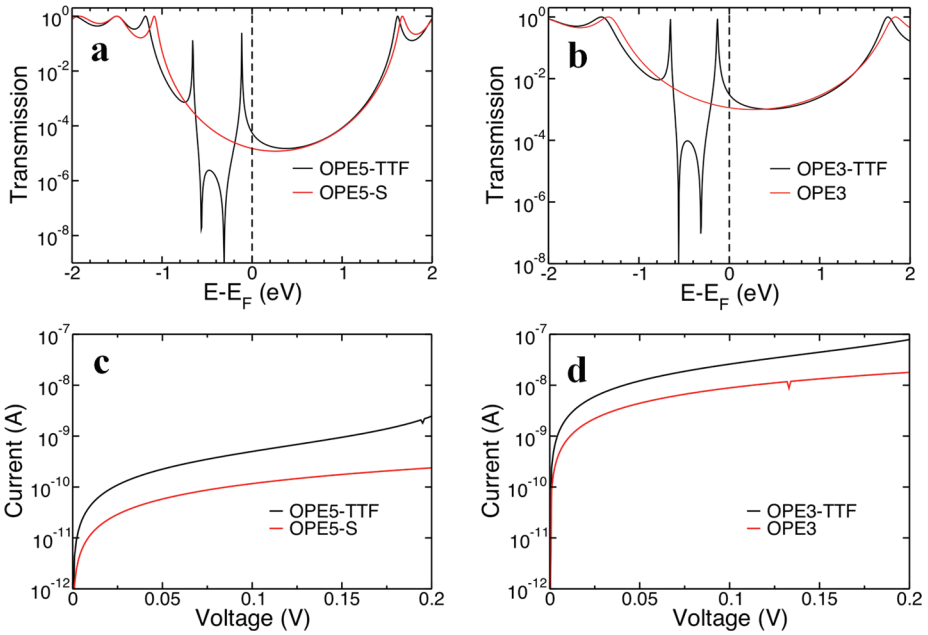

Figure 5. Calculated (a, b) transmission and (c, d) current through the four OPEs showing that the single-molecule calculations reproduce the result that the TTF substituents result in a significant increase in the current.

OPE3). The optical energy gaps (E_g) calculated from the edge of UV−vis absorption of OPEs also show a similar trend (Table S1, Supporting Information). UV−vis (Figure S2, Supporting Information) shows that the main peak belonging to the OPE backbone does not change much as a result of the different side substituents. However, the appearance of TTF peaks makes the edges of OPE5−TTF and OPE3−TTF absorptions red shift about 95 and 115 nm, respectively. These results imply that OPE5−TTF (or OPE3−TTF) have smaller HOMO−LUMO gaps than OPE5-S (or OPE3).

It has been reported that for short molecular wires[5,17,21] the exponential increase in resistance is consistent with the nonresonant tunneling process, described by eq 1

$$R = R_0 \exp(\beta l) \quad (1)$$

where R is the junction resistance, R_0 is the effective contact resistance, β is the tunneling attenuation factor, and l is the molecular length. A linear fit of resistance versus molecular length in the OPE SAMs junctions (Figure S5, Supporting Information) was set into two groups: OPE5−TTF and OPE3−TTF (with TTF substituents), OPE5-S, and OPE3 (without TTF substituents). The molecular length was calculated by DFT (Table S2, Supporting Information) and defined the S−S distance in the optimized structure. Two similar β values were obtained from linear fits of the data, 1.96 and 2.01 nm^{-1} for the OPEs with and without TTF substituents, respectively. These two values were within the range of values observed in typical conjugated systems,[15,17] and the relatively high β implied that a tunneling process is taking place in our SAM junctions. The similar value of β most likely arises from the nature of the same anchor group (S−Au). However, the obtained effective contact resistances were about 1 order of magnitude different. For OPEs with TTF substituents R_0 was 2.25 × 10^4 Ω. For OPEs without TTF substituents, R_0 was much higher and calculated to be 1.74 × 10^5 Ω. The TTF groups change the molecular energy gaps and alignment of the gaps to the electrode Fermi level, providing the difference in effective contact resistances. Lower contact resistance is beneficial for an efficient charge transport in the junctions and induces lower junction resistances.

Because the Pt/Cr-coated conductive tips were used as the top electrode in these experiments and the atomic structure of the Au−SAM/Pt interface is not clearly resolved, the problem is further simplified by considering the individual molecules chemisorbed between two Au electrodes for the transport calculations.[40] The optimized molecules were chemisorbed to an FCC hollow site on two gold (111) electrodes with the terminal hydrogen atoms removed and the Au−S bond length taken from the literature.[46] We calculated the transport using gDFTB[47−51] with no gold atoms included in the extended molecule. We integrated the bias-dependent transmission over an energy window, the size of which is controlled by the magnitude of the applied bias, in order to obtain the current through the system. As the molecules are symmetrically bound to the two electrodes in the transport calculations, we assume that the applied bias drops symmetrically across the junction, a further point of departure from the measured systems. While transmission is not an experimental observable, it shows the features that control the magnitude of the current through the molecules, and thus, we plot both transmission and predicted $I-V$ curves. We plot transmission versus energy relative to the Au Fermi energy (here set to −5.0 eV). These results are shown in Figure 5, clearly reproducing the experimental finding that in both cases the TTF substituent results in an increase in the current.

It is interesting to note from the calculated transmission that the TTF substituents introduce both additional resonant peaks and destructive interference dips. The gold Fermi energy used in these calculations is closer to a peak resulting in the increased current through the TTF-substituted molecules; however, this need not be the same for other kinds of electrode materials. Compared with the experimental results the ratios for the current are somewhat reduced; at 0.1 V the conductance of TTF-substituted systems were 4.27 and 2.93 times higher for the OPE5 and OPE3 systems, respectively (Figure 5c and 5d). From the transmission it is clear that this

dx.doi.org/10.1021/la204340n | *Langmuir* 2012, 28, 4016−4023

ratio is going to be very sensitive to the position of the Fermi energy, which is a parameter in these calculations, and the exact correspondence with experiment is unknown. Given the differences between theory and experiment in the nature of the electrodes, only qualitative agreement can be expected. Previously,[40] we have seen good qualitative agreement between single-molecule calculations of this kind and monolayer transport measurements (in that case with an EGaIn top contact); again, here the results suggest that interactions within the monolayer do not dominate the transport characteristics, and consequently, the single molecule calculations can reproduce the trends. The intermolecular action could increase the electrical conductance of molecular junctions by the chain-to-chain pathway tunneling under applied loading force of CP-AFM.[15,52,53] With the large conjugated TTF side chains, OPE5−TTF and OPE3−TTF may have stronger intermolecular $\pi-\pi$ stacking than OPE5-S and OPE3. Although the "through-bond" interactions appear to dominate the transport in these molecular junctions, the higher conductance of OPE5−TTF and OPE3−TTF monolayer junctions might also benefit from the higher intermolecular actions.

A recent theoretical study by Leijnse et al.[54] points to the possibility of observing NDR in asymmetric molecular junctions of, e.g., OPE−TTF cruciforms. However, we did not observe this phenomenon within our currently applied experimental voltage range.

CONCLUSION

We fabricated high-quality SAMs of OPEs on ultraflat gold substrates. Cruciform oligo(phenylene ethynylene)s (OPEs) with an extended tetrathiafulvalene (TTF) donor substitute group (OPE5−TTF and OPE3−TTF) and their simple analogues (OPE5-S and OPE3) without conjugated substituent were used. Molecular junctions based on these SAMs were investigated using conducting probe-atomic force microscopy. The TTF substituent changes the molecular orbital energy levels and decreases the energy gap and contact resistance of the molecular junction, resulting in an increase of the conductance by a factor of about 10 for the OPE5s and OPE3s. Quantum chemical calculations of the transmission qualitatively agreeing with the experimental data implied that the "through-bond" interactions dominated the transport in these molecular junctions.

EXPERIMENTAL SECTION

Ultraflat Gold Substrates. Ultraflat gold substrates were made by an annealed template stripping approach, modified from the methods of Whitesides[41] and Pinkhassik[42] et al. Two hundred nanometer gold films were deposited by e-gun evaporation at a rate of 0.2 nm/s (1×10^{-7} Torr) onto freshly cleaned atomically flat Si/SiO_2 templates and then annealed at 100 °C (we tried with several different temperatures and finally found that 100 °C annealed samples were the flattest, see Supporting Information) under N_2 for 1 h. After applying a 5 $\mu L/cm^2$ drop of Epo-Tek 353ND (Precision Fiber Products Inc.) to the gold surface, another similar sized silicon wafer was placed face down covering it without any additional applied pressure and the Epo-Tek spread over the entire gold film by the weight of upper silicon wafer. The sandwich structure was heated at 120 °C for 20 min under atmosphere to cure the Epo-Tek glue. The silicon wafer/Epo-Tek/gold structure was stripped from the Si/SiO_2 template by gently using a thin blade around the edge of the interface between the gold and the template. The ultraflat gold surface which was induced by the atomically flat Si/SiO_2 template was exposed and showed a small average roughness of 0.2−0.3 nm (see Supporting Information). Unstripped sandwich structures could be stored for a long time without any contamination on gold films.

Formation of SAMs. OPE molecules (OPE5−TTF and OPE3−TTF were synthesized as previously reported;[31] syntheses of OPE5-S and OPE3−TTF are described in the Supporting Information; OPE3 was purchased from Sigma-Aldrich) were dissolved at 0.25 mM in 15% triethylamine (Et_3N) in THF (as reported by Chiechi et al.[34,40]) which had been purged of O_2 with a steady flow of Ar. Freshly stripped ultraflat gold substrates were immediately immersed into the solutions. The containers were filled with Ar and sealed and then left with the absence of light for 48 h at room temperature to grow the SAMs. After removal from the solutions, all samples were extensively rinsed with THF and ethanol and then dried under a stream of N_2 before all measurements.

Measurements. AFM images and CP-AFM measured electrical properties were obtained using a Digital Instruments Nanoscope III at room temperature in air.[55] For CP-AFM, Pt/Cr-coated conductive tapping mode tips (BudgetSensors Inc.) were used. The current−voltage ($I-V$) characteristics of the SAMs were measured by combining an AFM, a Keithley 2400 digital source meter, a Keithley 6154 power source, and an input control and output recording program with Labview. The conductive tip in contact with SAMs was the top electrode, and the stripped Au substrate at the bottom of the SAM was connected with a conducting wire as one external electrode. For each group of OPEs, $I-V$ curves were recorded using the same tip and at least 5 different places (5 cyclic measurements at each place) for each SAM. Conventional cyclic voltammetry measurements were carried on a BiStat BioLogic Science Instrument with EC-Lab using a three-electrode cell contain a Au work electrode (~0.4 cm^2), a platinum electrode, and a Ag/AgCl reference electrode in 5.0 mM $K_3Fe(CN)_6/K_4Fe(CN)_6$ solution with 1 M KNO_3 as supporting electrolyte. XPS experiments were performed in a Kratos Axis Ultra^{DLD} fitted with a monochromated Al Kα ($h\nu$ = 1486.6 eV, power = 150 W) X-rays source. The base pressure in the chamber was 5×10^{-10} mbar and never exceeds 5×10^{-9} mbar during an experiment. A pass energy (PE) of 160 eV was used for a wide scan and PE = 10 eV for a high-resolution scan. Data were analyzed with the software casaXPS. All samples were energy calibrated using the Au $4f_{7/2}$ line at 84 eV.

Quantum Chemical Calculation. The structures of the isolated molecules were optimized using density functional theory with the B3LYP functional and the 6-311g** basis set in Q-Chem.[45] Optimized molecules then chemisorbed to an FCC hollow site on two gold (111) electrodes with the terminal hydrogen atoms removed and the Au−S bond length taken from the literature.[46] The transport properties were calculated using gDFTB[47−51] with no gold atoms included in the extended molecule. The molecular energy orbitals for the isolated molecules were calculated with the smaller 6-3 g* basis.

ASSOCIATED CONTENT

Supporting Information

Experimental details for the ultraflat gold substrate films, UV−vis absorption spectra, optimized molecular structures and energy gaps, SAM thickness and DFT length of the four OPEs, calibration of $I-V$ measurements, plot of resistance versus molecular length, AFM images of the SAMs, and synthesis of OPE5-S and OPE3−TTF. This material is available free of charge via the Internet at http://pubs.acs.org.

AUTHOR INFORMATION

Corresponding Author

*E-mail: kn@nano.ku.dk (K.N.); bwl@nano.ku.dk (B.W.L.).

Notes

The authors declare no competing financial interest.

ACKNOWLEDGMENTS

This work was supported by The Danish-Chinese Center for Molecular Nanoelectronics funded by the Danish National

Research Foundation, the European Community Seventh Framework Program under grant agreement no. 270369 "ELFOS", and the National Natural Science Foundation of China (60911130231). We are grateful to Prof. Susan Stipp and Dr. Tue Hassenkam for fruitful discussions. Finally, we acknowledge the Danish Government funded UNIK Synthetic Biology program.

REFERENCES

(1) Aviram, A.; Ratner, M. A. *Chem. Phys. Lett.* **1974**, *29*, 277−283.
(2) Osorio, E. A.; Bjørnholm, T.; Lehn, J.-M.; Ruben, M.; van der Zant, H. S. J. *J. Phys.: Condens. Matter* **2008**, *20*, 374121.
(3) McCreery, R. L.; Bergren, A. J. *Adv. Mater.* **2009**, *21*, 4303−4322.
(4) Moth-Poulsen, K.; Bjørnholm, T. *Nat. Nanotechnol* **2009**, *4*, 551−556.
(5) Song, H.; Reed, M. A.; Lee, T. *Adv. Mater.* **2011**, *23*, 1583−1608.
(6) Lindsay, S. M.; Ratner, M. A. *Adv. Mater.* **2007**, *19*, 23−31.
(7) Li, T.; Hu, W.; Zhu, D. *Adv. Mater.* **2010**, *22*, 286−300.
(8) Hines, T.; Diez-Perez, I.; Hihath, J.; Liu, H.; Wang, Z.-S.; Zhao, J.; Zhou, G.; Müllen, K.; Tao, N. *J. Am. Chem. Soc.* **2010**, *132*, 11658−11664.
(9) Martin, C. A.; Ding, D.; Sørensen, J. K.; Bjørnholm, T.; van Ruitenbeek, J. M.; van der Zant, H. S. J. *J. Am. Chem. Soc.* **2008**, *130*, 13198−13199.
(10) Kubatkin, S.; Danilov, A.; Hjort, M.; Cornil, J.; Brédas, J.-L.; Stuhr-Hansen, N.; Hedegård, P.; Bjørnholm, T. *Nature* **2003**, *425*, 698−701.
(11) Choi, S. H.; Kim, B.; Frisbie, C. D. *Science* **2008**, *320*, 1482−1486.
(12) Thuo, M. M.; Reus, W. F.; Nijhuis, C. A.; Barber, J. R.; Kim, C.; Schulz, M. D.; Whitesides, G. M. *J. Am. Chem. Soc.* **2011**, *133*, 2962−2975.
(13) Nijhuis, C. A.; Reus, W. F.; Whitesides, G. M. *J. Am. Chem. Soc.* **2010**, *132*, 18386−18401.
(14) Akkerman, H. B.; Boer, B. d. *J. Phys.: Condens. Matter* **2008**, *20*, 013001.
(15) Salomon, A.; Cahen, D.; Lindsay, S.; Tomfohr, J.; Engelkes, V. B.; Frisbie, C. D. *Adv. Mater.* **2003**, *15*, 1881−1890.
(16) Engelkes, V. B.; Beebe, J. M.; Frisbie, C. D. *J. Am. Chem. Soc.* **2004**, *126*, 14287−14296.
(17) Choi, S. H.; Frisbie, C. D. *J. Am. Chem. Soc.* **2010**, *132*, 16191−16201.
(18) Choi, S. H.; Risko, C.; Delgado, M. C. R.; Kim, B.; Brédas, J.-L.; Frisbie, C. D. *J. Am. Chem. Soc.* **2010**, *132*, 4358−4368.
(19) Bumm, L. A.; Arnold, J. J.; Cygan, M. T.; Dunbar, T. D.; Burgin, T. P.; Jones, L.; Allara, D. L.; Tour, J. M.; Weiss, P. S. *Science* **1996**, *271*, 1705−1707.
(20) Tour, J. M.; Kozaki, M.; Seminario, J. M. *J. Am. Chem. Soc.* **1998**, *120*, 8486−8493.
(21) Lu, Q.; Liu, K.; Zhang, H.; Du, Z.; Wang, X.; Wang, F. *ACS Nano* **2009**, *3*, 3861−3868.
(22) Leary, E.; Higgins, S. J.; van Zalinge, H.; Haiss, W.; Nichols, R. J. *Chem. Commun.* **2007**, 3939−3941.
(23) Venkataraman, L.; Park, Y. S.; Whalley, A. C.; Nuckolls, C.; Hybertsen, M. S.; Steigerwald, M. L. *Nano Lett.* **2007**, *7*, 502−506.
(24) Baheti, K.; Malen, J. A.; Doak, P.; Reddy, P.; Jang, S.-Y.; Tilley, T. D.; Majumdar, A.; Segalman, R. A. *Nano Lett.* **2008**, *8*, 715−719.
(25) (a) Grunder, S.; Huber, R.; Horhoiu, V.; González, M. T.; Schönenberger, C.; Calame, M.; Mayor, M. *J. Org. Chem.* **2007**, *72*, 8337−8344. (b) Grunder, S.; Huber, R.; Wu, S.; Schönenberger, C.; Calame, M.; Mayor, M. *Eur. J. Org. Chem.* **2010**, 833−845.
(26) Chen, J.; Reed, M. A.; Rawlett, A. M.; Tour, J. M. *Science* **1999**, *286*, 1550−1552.
(27) Donhauser, Z. J.; Mantooth, B. A.; Kelly, K. F.; Bumm, L. A.; Monnell, J. D.; Stapleton, J. J.; Price, D. W.; Rawlett, A. M.; Allara, D. L.; Tour, J. M.; Weiss, P. S. *Science* **2001**, *292*, 2303−2307.
(28) Xiao, X.; Nagahara, L. A.; Rawlett, A. M.; Tao, N. *J. Am. Chem. Soc.* **2005**, *127*, 9235−9240.
(29) Huber, R.; González, M. T.; Wu, S.; Langer, M.; Grunder, S.; Horhoiu, V.; Mayor, M.; Bryce, M. R.; Wang, C.; Jitchati, R.; Schönenberger, C.; Calame, M. *J. Am. Chem. Soc.* **2008**, *130*, 1080−1084.
(30) Liao, J.; Agustsson, J. S.; Wu, S.; Schönenberger, C.; Calame, M.; Leroux, Y.; Mayor, M.; Jeannin, O.; Ran, Y.-F.; Liu, S.-X.; Decurtins, S. *Nano Lett.* **2010**, *10*, 759−764.
(31) Jennum, K.; Vestergaard, M.; Pedersen, A. H.; Fock, J.; Jensen, J.; Santella, M.; Led, J. J.; Kilså, K.; Bjørnholm, T.; Nielsen, M. B. *Synthesis* **2011**, 539−548.
(32) Sørensen, J. K.; Vestergaard, M.; Kadziola, A.; Kilså, K.; Nielsen, M. B. *Org. Lett.* **2006**, *8*, 1173−1176.
(33) Vestergaard, M.; Jennum, K.; Sørensen, J. K.; Kilså, K.; Nielsen, M. B. *J. Org. Chem.* **2008**, *73*, 3175−3183.
(34) Valkenier, H.; Huisman, E. H.; van Hal, P. A.; de Leeuw, D. M.; Chiechi, R. C.; Hummelen, J. C. *J. Am. Chem. Soc.* **2011**, *133*, 4930−4939.
(35) Issac, Y. A.; Elzein, S. M.; Barakat, Y. *Rev. Roum. Chim.* **1995**, *40*, 463−470.
(36) Cram, D. J.; Daeniker, H. U. *J. Am. Chem. Soc.* **1954**, *76*, 2743−2752.
(37) Zhang, W.; Moore, J. S. *Macromolecules* **2004**, *37*, 3973−3975.
(38) Onitsuka, K.; Fujimoto, M.; Kitajima, H.; Ohshiro, N.; Takei, F.; Takahashi, S. *Chem.—Eur. J.* **2004**, *10*, 6433−6446.
(39) Yatabe, T.; Suzuki, Y.; Kawanishi, Y. *J. Mater. Chem.* **2008**, *18*, 4468−4477.
(40) Fracasso, D.; Valkenier, H.; Hummelen, J. C.; Solomon, G. C.; Chiechi, R. C. *J. Am. Chem. Soc.* **2011**, *133*, 9556−9563.
(41) Weiss, E. A.; Chiechi, R. C.; Kaufman, G. K.; Kriebel, J. K.; Li, Z.; Duati, M.; Rampi, M. A.; Whitesides, G. M. *J. Am. Chem. Soc.* **2007**, *129*, 4336−4349.
(42) Banner, L. T.; Richter, A.; Pinkhassik, E. *Surf. Interface Anal.* **2009**, *41*, 49−55.
(43) Liu, K.; Li, G.; Wang, X.; Wang, F. *J. Phys. Chem. C* **2008**, *112*, 4342−4349.
(44) Halik, M.; Hirsch, A. *Adv. Mater.* **2011**, *23*, 2689−2695.
(45) Shao, Y.; Molnar, L. F.; Jung, Y.; Kussmann, J.; Ochsenfeld, C.; Brown, S. T.; Gilbert, A. T. B.; Slipchenko, L. V.; Levchenko, S. V.; O'Neill, D. P.; DiStasio, R. A. Jr; Lochan, R. C.; Wang, T.; Beran, G. J. O.; Besley, N. A.; Herbert, J. M.; Yeh Lin, C.; Van Voorhis, T.; Hung Chien, S.; Sodt, A.; Steele, R. P.; Rassolov, V. A.; Maslen, P. E.; Korambath, P. P.; Adamson, R. D.; Austin, B.; Baker, J.; Byrd, E. F. C.; Dachsel, H.; Doerksen, R. J.; Dreuw, A.; Dunietz, B. D.; Dutoi, A. D.; Furlani, T. R.; Gwaltney, S. R.; Heyden, A.; Hirata, S.; Hsu, C.-P.; Kedziora, G.; Khalliulin, R. Z.; Klunzinger, P.; Lee, A. M.; Lee, M. S.; Liang, W.; Lotan, I.; Nair, N.; Peters, B.; Proynov, E. I.; Pieniazek, P. A.; Min Rhee, Y.; Ritchie, J.; Rosta, E.; David Sherrill, C.; Simmonett, A. C.; Subotnik, J. E.; Lee Woodcock Iii, H.; Zhang, W.; Bell, A. T.; Chakraborty, A. K.; Chipman, D. M.; Keil, F. J.; Warshel, A.; Hehre, W. J.; Schaefer Iii, H. F.; Kong, J.; Krylov, A. I.; Gill, P. M. W.; Head-Gordon, M. *Phys. Chem. Chem. Phys.* **2006**, *8*, 3172−3191.
(46) Bilic, A.; Reimers, J. R.; Hush, N. S. *J. Chem. Phys.* **2005**, *122*, 094708.
(47) Elstner, M.; Porezag, D.; Jungnickel, G.; Elsner, J.; Haugk, M.; Frauenheim, T.; Suhai, S.; Seifert, G. *Phys. Rev. B* **1998**, *58*, 7260.
(48) Frauenheim, T.; Seifert, G.; Elsterner, M.; Hajnal, Z.; Jungnickel, G.; Porezag, D.; Suhai, S.; Scholz, R. *Phys. Status Solidi B* **2000**, *217*, 41−62.
(49) Frauenheim, T.; Seifert, G.; Elstner, M.; Niehaus, T.; Koehler, C.; Amkreutz, M.; Sternberg, M.; Hajnal, Z.; Di Carlo, A.; Suhai, S. *J. Phys.: Condens. Matter* **2002**, *14*, 3015−3047.
(50) Porezag, D.; Frauenheim, T.; Köhler, T.; Seifert, G.; Kaschner, R. *Phys. Rev. B* **1995**, *51*, 12947.
(51) Pecchia, A.; Carlo, A. D. *Rep. Prog. Phys.* **2004**, *67*, 1497−1561.
(52) Fang, L.; Park, J. Y.; Ma, H.; Jen, A. K. Y.; Salmeron, M. *Langmuir* **2007**, *23*, 11522−11525.
(53) Song, H.; Lee, H.; Lee, T. *J. Am. Chem. Soc.* **2007**, *129*, 3806−3807.

(54) Leijnse, M.; Sun, W.; Nielsen, M. B.; Hedegård, P.; Flensberg, K. *J. Chem. Phys.* **2011**, *134*, 104107.
(55) Tang, Q.; Tong, Y.; Jain, T.; Hassenkam, T.; Wan, Q.; Moth-Poulsen, K.; Bjørnholm, T. *Nanotechnology* **2009**, *20*, 245205.